Cement and Concrete Research 168 (2023) 107149

Contents lists available at ScienceDirect

Cement and Concrete Research

journal homepage: www.elsevier.com/locate/cemconres

The "mica crisis" in Donegal, Ireland – A case of internal sulfate attack?

Andreas Leemann [a,b,*], Barbara Lothenbach [a,c], Beat Münch [a], Thomas Campbell [d], Paul Dunlop [b]

[a] Empa, Laboratory for Concrete & Asphalt, Überlandstrasse 129, CH-8600 Dübendorf, Switzerland
[b] School of Geography and Environmental Sciences, Ulster University, Coleraine BT52 1SA, Northern Ireland, UK
[c] NTNU, Department of Structural Engineering, Trondheim, Norway
[d] TA Group, Kiltimagh, F12 Y6V0, Ireland

ARTICLE INFO

Keywords:
Concrete
Pyrrhotite
Internal sulfate attack
Microstructure
Cracking

ABSTRACT

In County Donegal, northwest Ireland, thousands of homes built with concrete blocks show an increasing degree of severe structural defects attributed to high mica content in the aggregates. Consequently, the problem is popularly known as the "Mica Crisis". In this project the concrete blocks of four affected homes are investigated by microstructural and chemical analysis combined with thermodynamic modelling.

Apart from mica, the aggregates contain iron sulphides mainly in the form of pyrrhotite. The sulfur content of the aggregates considerably exceeds the limit value defined by the European standard for concrete aggregates (EN 12620). The results of the microstructural analysis coupled with thermodynamic modelling demonstrate that the concrete suffers from internal sulfate attack triggered by pyrrhotite oxidation. The comparison of the results of this investigation with the data collected by chartered engineers on almost hundred damaged homes shows that the four investigated cases are representative of the situation in Donegal.

1. Introduction

Concrete blocks are widely used for building homes in the Republic of Ireland. These homes are typically built on concrete foundations with the structure containing an outer leaf of concrete blocks that has a plaster render to protect it, an inner leaf and an insulation layer in between. Homes in west and northwest Ireland built this way from the late 1990's onwards are increasingly affected by severe cracking. In the northwest in County Donegal, homes have been widely exhibiting structural distress in the form of web-like cracking on external walls since 2013. The degree of deterioration, in the now estimated five thousand affected homes, ranges from cracking running through the blocks and their render perpendicular to their surface, to complete disintegration and strength loss leading to severe structural damage. The same type of damage is observed on numerous commercial properties and public buildings.

In 2016, the government appointed a panel to investigate the issue. After a desktop review, they determined that the damage was likely caused by excessive levels of muscovite mica in the aggregates making the blocks vulnerable to frost damage or damage by wetting-drying cycles due to weather changes [1]. This assumption however has not been confirmed by scientific evidence to date and as such, should be regarded as an unproven hypothesis. In 2022, the government introduced a €3 billion grant scheme to assist homeowners. To qualify, engineers must investigate the homes using the National Standards Authority of Ireland (NSAI) document I·S. 465:2018 + A1:2020 (herein referred to as I.S. 465) [2]. This includes a damage assessment report informed by petrographic analysis of concrete samples. The major source of the aggregates used in defective concrete blocks in Donegal contains mica-rich phyllite and schist quarried from Dalradian metamorphic formations. However, petrographic analysis completed on the majority of Donegal homes investigated to date following I.S 465 has found clear evidence of iron sulfides, mainly in the form of pyrrhotite. Oxidizing iron sulfides in combination with internal sulfate attack can lead to severe concrete deterioration [3–7]. Concrete foundations of thousands of homes in the Trois Rivières region in Canada [8–13] and in Connecticut and Massachusetts in the US [14–16] have been damaged by this type of attack.

Identifying the damage mechanism in the Irish concrete blocks is extremely important for the success of the entire scheme. However, despite its occurrence and the known risks, pyrrhotite is currently not taken into consideration when deciding on one of the five remediation options available within I.S. 465 that range from removing the outer leaf, through to full demolition and rebuild. All but the latter option

* Corresponding author at: Empa, Laboratory for Concrete & Asphalt, Überlandstrasse 129, CH-8600 Dübendorf, Switzerland.
E-mail address: andreas.leemann@empa.ch (A. Leemann).

https://doi.org/10.1016/j.cemconres.2023.107149
Received 3 November 2022; Received in revised form 11 January 2023; Accepted 5 March 2023

means that existing blockwork containing pyrrhotite is preserved and could potentially fail in the future. Therefore, effective remediation options have to be based on fully understood damage mechanisms. This has important implications for government finances too, as partially remediated homes that subsequently fail can access the grant scheme for a second time. This could substantially increase the financial burden on the state in the long term adding to an already expensive scheme.

The goal of this study is to identify the reasons for the failure of the concrete blocks in Donegal. An in-depth microstructural analysis of the concrete blocks from four affected homes with a characterization of the cement hydrate assemblage performed using scanning electron microscopy (SEM) with energy-dispersive X-ray spectroscopy (EDS) is performed. Additionally, the mineralogy of the concrete is studied with X-ray diffraction (XRD) and the content of sulfur in the concrete present as sulfide is determined. Moreover, thermodynamic modelling within the boundary conditions established by SEM and EDS is performed.

2. Materials and methods

2.1. Materials

The mix design of the concrete used for block production is unknown and may vary between producers. The blocks are pressed into their forms and are available in different sizes. A commonly used block size is 440 × 215 × 100 cm^3 (commonly called 'a 4″ block'). The required characteristic compressive strength is 7.5 MPa [17,18].

The four investigated homes are located in the Inishowen Peninsula in North Donegal. All homes were built between 2001 and 2004 and for all the decision to demolish them was taken by a Chartered Engineer who followed the I.S. 465 protocols. The homes showed the typical signs of distress associated with defective concrete blocks and displayed patterned cracking on the external leaf, with cracks typically ranging in width from 1 mm up to 16 mm. Homes A and D also had large sections of exposed concrete blocks that easily disintegrated when pressed by hand. As only cores were extracted from the four affected homes, the dimensions of the blocks are not known, however they are likely to be standard block size mentioned above. Cores with a diameter of 100 mm were taken by dry coring. The length of the cores is given by the thickness of the blocks and corresponds to 100 mm (Fig. 1). However, the actual diameter and length can be smaller due to mechanical erosion during coring that is the result of the low-strength cement paste. More detailed information on the specific samples is given below.

Previous to this study, the four homes were already investigated to access to the government grant scheme and these data are available from Chartered Engineer reports. Results of these reports are presented in the supplementary data. Additionally, some key findings of a data collection of 91 homes are reported as well in the supplementary data.

2.1.1. Home A, built 2004

The east facing wall of the ground floor shows extensive cracking in both vertical and horizontal directions, with cracks ranging in width from 1 mm to 15 mm. In areas where the plaster has spalled, the exposed concrete blocks experience granular disintegration and aggregate can be easily scraped by hand from the blocks. Two coring locations were attempted on the ground floor at this property. The first was in an area where the render had spalled and the exposed blocks were disintegrating. It was not possible to retrieve an intact core at this location due to the concrete continually disintegrating in the core bit (Sample A1). Another sample was therefore taken 40 cm away from Sample A1 on a section of the wall that was still covered with render. Here an intact core was recovered (Sample A2, Fig. 1).

2.1.2. Home D, built 2002

Sample D1 was taken from the west facing wall of the ground floor (Fig. 2) which is heavily cracked, with cracks of up to 16 mm wide observed both here and on all four elevations of the house. In areas where the plaster has spalled exposing the blocks, all blocks experience granular disintegration and can be easily broken by hand. In these locations, it was not possible to take a core and pieces of the disintegrating blocks were collected by hand (sample D1). The concrete at this location was directly exposed to rain. In an area of the same wall where the plaster was still intact, it was possible to extract a core between the cracks (sample D2) (Fig. 2).

2.1.3. Home E, built 2001

Cores from both the inner and outer leaf were taken from the ground floor on the north, south, east and west facing outer and inners walls of this home. The cores were taken by coring through the outer leaf, across the cavity and through the internal leaf. At each sample location, an area of the outer leaf that had a 1–2 mm width crack was targeted for sampling. The corer was positioned on the center of the crack line to ensure the damaged part was captured in the sample. An inspection of the internal walls at this property confirmed that the inner leaf had no cracks, so the four inner leaf samples were taken from walls that showed no obvious visual signs of distress. A core taken from the south facing outside gable wall was chosen for microscopy. The outer leaf of this wall displayed extensive web-like cracking throughout, with cracks ranging in width from 1 mm to 10 mm. Four different sample locations were tried on this wall to obtain a sample as the concrete disintegrated during coring. The extracted concrete samples from the outer leaf were quite soft and easy to break by hand. The entire cross-section of the cores showed this low strength. There were no parts with higher strength, like the side of the concrete block that was in contact with the insolation layer inside the cavity.

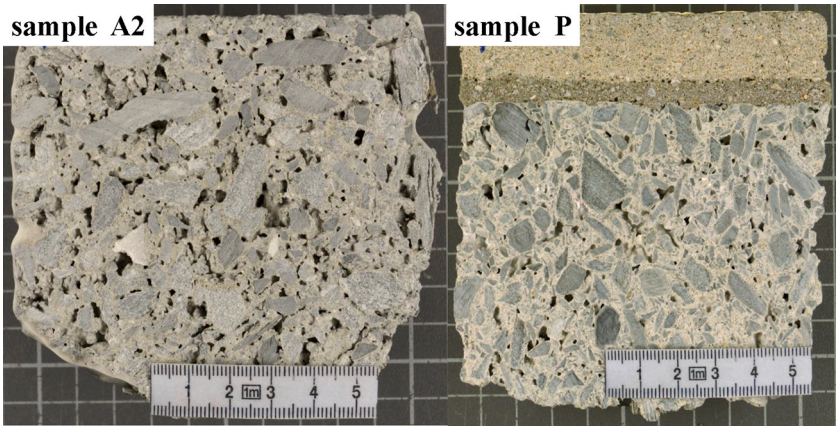

Fig. 1. Cores from homes A and P cut along their length axis. The plaster of home A fell off during cutting.

Fig. 2. Locations of sample extraction in home D. Note the serious structural damage to the right side of this home.

2.1.4. Home P, built 2005

The cores from this home were extracted from the west facing gable wall on the ground floor. The wall shows vertical and horizontal cracks, from 1 mm to 5 mm in width. The core was taken on a location with only one minor 1-mm wide width crack. The concrete retrieved in the core was strong and it was not possible to break it apart by hand (Fig. 1).

From each sample, a piece of about 100 g was broken off and crushed to a size of <1.0 mm. Subsequently, the samples were ground for the determination of the iron sulfide content.

From each home, three samples from the outer leaf were cut or broken to a size fitting into a cylinder with a diameter of 50 mm. During cutting of the samples, it was evident that the low concrete strength of

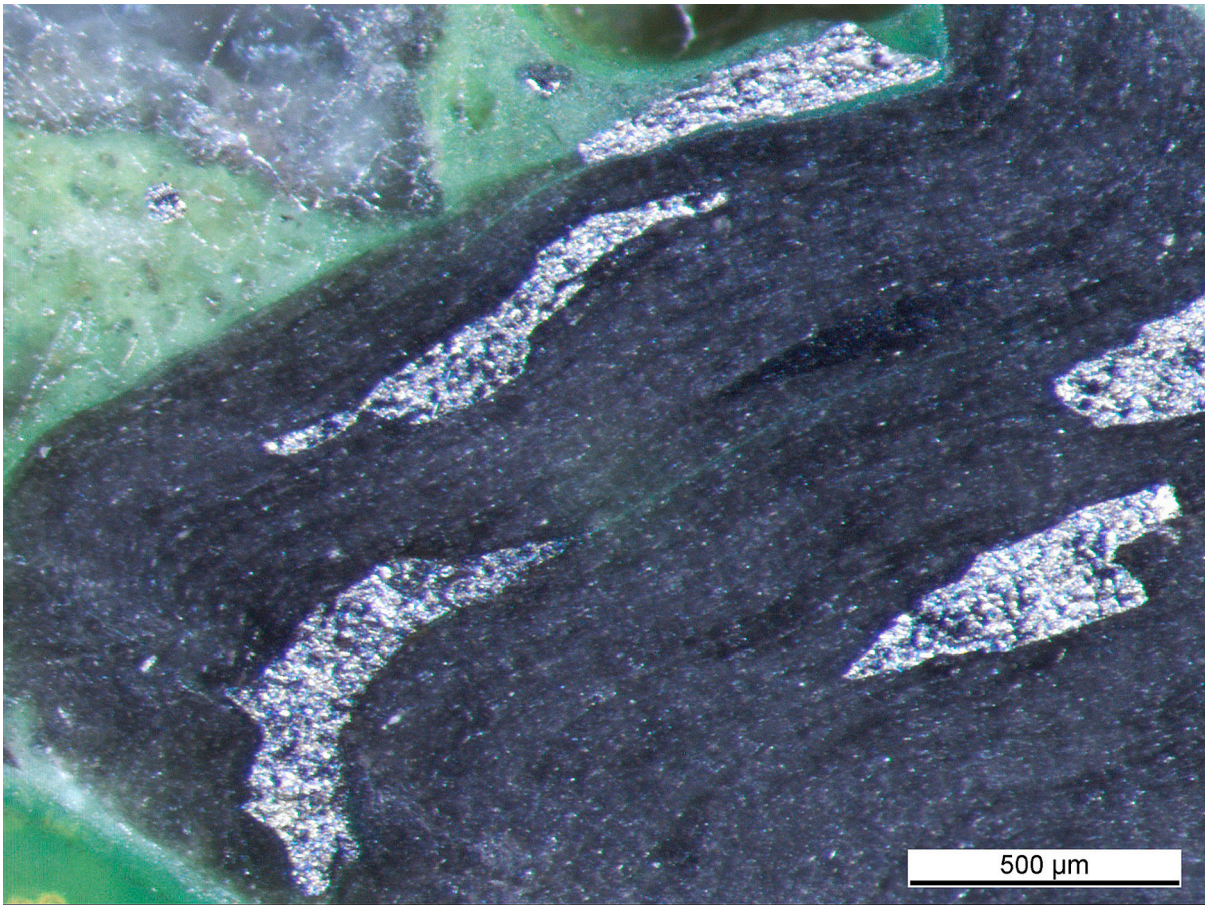

Fig. 3. Iron sulfides/bright elongated particles) in phyllite aggregate after grinding in sample P. Polished section under the optical microscope.

samples A, D and E applied to the entire length of the cores and cross-section of the blocks, respectively. There was no difference in the tendency of the concrete to disintegrate during cutting between the part of the core in contact with the external render or the part in contact with the insulation. Two samples from the inner leaf of home E were prepared. In contrast to the samples of the outer leaf, these samples exhibited no disintegration during cutting. After drying for 24 h at 50 °C, the samples were pressure impregnated with epoxy resin, embedded in the cylinders, ground and polished. Iron sulfides were easily identified under the optical microscope after grinding (Fig. 3). It has to be noted that brownish iron hydroxide ($Fe(OH)_3$) indicating iron sulfide oxidation was absent in home P and only very few aggregate particles showed this in the samples E, A2 and D2. The largest number of particles with brownish iron hydroxides was present in the completely disintegrated samples of homes A1 and D1. Four samples per core were cut for the investigation with the SEM (samples A2, D2, E and P). Two samples always included a small section of the plaster, if it was still present. The other two samples were cut from the part of the outer leaf formerly in contact with the insulation. In the case of the completely disintegrated concrete (samples A1 and D1) four larger pieces fitting into the container used for epoxy impregnation (cylinder with a diameter of 50 mm) were selected. All samples were dried in an oven for three days at 40 °C, impregnated with epoxy resin, polished and carbon coated. The final samples have a disc-shape and measure 50 mm in diameter. In addition to the polished sections, a polished thin section was produced from each home. This permitted an investigation of the same samples with both optical and scanning electron microscopes.

The fines (< 1 mm) of the completely disintegrated concrete (samples A1 and D1) were crushed, homogenized and ground by hand to a particle size of <63 μm using an agate mortar for analysis with XRD. Only the fines were selected to possibly identify some components of the cement paste that are expected to be enriched in this grain size.

2.2. Methods

2.2.1. Experimental

Sulfide was determined according to DIN EN 196-2:2013 [19], section 4.4.5. The sample was treated with hydrochloric acid under reducing condition, and the formed gaseous hydrogen sulfide was precipitated as zinc sulfide by means of an ammoniacal solution of zinc sulfate. The amount of precipitated zinc sulfide was determined by iodometry.

Total sulfate was determined according to DIN EN 196-2:2013 [19], section 4.4.2 by dissolving the sample in hydrochloric acid. The sulfate was precipitated with barium chloride as barium sulfate and determined gravimetrically.

Water soluble sulfate was determined according to EN 1744-1, section 10 [20]. The sample was digested with deionized water. Sulfate was determined gravimetrically as barium sulfate.

For image acquisition, a FEI Quanta 650 was used in the high vacuum mode (pressure of 3.5–5.0 × 10^{-6} Torr) employing an acceleration voltage of 12.5 kV, a spot size of 4.5 and a beam current of 155–170 μA. Images were acquired in the secondary-electron-mode (SE) and in the back-scattering-electron mode (BSE). EDS was conducted with a Thermo Noran Ultra Dry 60 mm^2 detector and Pathfinder X-Ray Microanalysis Software. For the single point analysis, the same setting as for image acquisition was employed using K-lines. Acceleration voltage and spot size were increased for element mappings to 20 kV and 5.0, respectively.

In order to analyze the composition of the cement paste, a magnification of 1500 to 3000 times was used so that small aggregate particles could be avoided as they may possibly interfere with the analysis (interaction volume of the electron beam). The points were placed in a way to obtain a representative composition of the cement paste at the chosen location where 20–80 points were analyzed. About 1000 EDS point analysis of the cement paste were conducted in total. The results of EDS point analysis are presented as atomic ratio plots. The size of cement hydrates is considerably smaller than the interaction volume below the point of beam incidence. As a result, the EDS spectrum is usually generated by several cement hydrates in unknown and variable quantities. For that reason, the results from EDS point analysis are presented as elemental ratio plots based on atom-%. This approach is well established in the EDS analysis of cementitious materials [21]. All values given in percentages relate to atomic-%.

Phase clustering of the element maps was performed based on the approach described in [22]. This procedure is based on an automated identification of the chemical compositions of phases followed by their clustering. This allows the occurrence of predefined phases and their spatial distribution at the investigated location to be shown.

XRD were performed using a PANalytical X'Pert Pro MPD diffractometer in a Θ-Θ configuration with CoKα radiation, a fixed divergence slit size of 0.5°, a rotating sample stage and the X'Celerator detector. The samples were measured for between 5° and 90° 2Θ using a total acquisition time of 90 min. A qualitative phase identification was performed using the X'Pert High Score Plus V. 4.9 software and the ICCD PDF-2 database.

The sheet silicates present in the samples are muscovite and chlorite. Chlorite does not belong to the mica group [23]. However, as in all the Chartered Engineer reports of the homes this distinction is not made and all sheet silicates are termed “mica”, this designation has been adopted for the paper.

2.2.2. Thermodynamic modelling

The composition of hydrated cements and the changes upon the interaction with the environment can be calculated by thermodynamic modelling, as has been demonstrated for many applications [24–29]. Thermodynamic modelling is carried out using the geochemical modelling code Gibbs Energy Minimization Selektor (GEMS) [30], which computes equilibrium phase assemblages and speciation in complex geochemical systems. The general thermodynamic data were selected from the PSI/Nagra thermodynamic database [31], complemented with solubility products for cement hydrates [32], zeolitic phases [33–35] and chlorite, represented by the Mg-rich endmember clinochlore, $Mg_5Al_2Si_3O_{10}(OH)_8$ [36]. The composition of calcium silicate hydrates (C-S-H) was modelled using the “CSHQ” model [37], which accounts for the uptake of alkali in the C-S-H phase [32]. The formation of quartz (SiO_2), dolomite ($CaMg(CO_3)_2$), goethite (FeOOH), hematite (Fe_2O_3) and of some zeolitic phases (natrolite, heulandite and stilbite) was suppressed in the calculations due to kinetic reasons. The calculations refer to the hydrate composition expected at 10 °C.

As the composition of the cement and the mix design of the concrete was not reported, a Portland cement (PC) containing 4 mass-% of calcite (the composition from [38] is detailed in Table 1) has been used to calculate the hydrate assemblage assuming water-to-cement ratio of 0.6. Based on the measured sulfide contents (see below), the presence of 10 g pyrrhotite (FeS) per 100 g unhydrated cement was assumed. FeS was allowed to react with oxygen if available.

3. Results

3.1. Sulfur content

The content of sulfur present as sulfides in the blocks ranges from 0.40 to 0.71 mass-% of the concrete (Table 2). These values are well above the limit value of ≤0.1 mass-% for aggregates containing pyrrhotite given by EN 12620 [39] and S.R. 16 [40].

3.2. X-ray diffraction

The composition of the fines in samples A1 and D1 are nearly identical (Fig. 4). They contain chlorite, muscovite, quartz, albite and traces of rutile as components of the aggregates. As further crystalline phase ankerite is identified (main reflection outside the displayed 2θ-range).

Table 1
Oxide composition of the Portland cement (PC) containing 4 mass-% of limestone used for the thermodynamic modelling (in mass-%) based on XRF data [38].

Component	SiO_2	Al_2O_3	Fe_2O_3	CaO	MgO	K_2O	Na_2O	SO_3	CO_2
Portland cement	19.4	4.7	3.1	63.5	1.8	0.7	0.4	2.2	1.9

Table 2
Content of sulfur present as sulfides in the concrete samples from the four homes. The coding for home E: the second letter indicates the geographic direction, the third indicates outer (O) or inner (I) leaf.

Home	A	D	P	E_{NI}	E_{NO}	E_{WI}	E_{WO}	E_{SI}	E_{SO}	E_{EI}	E_{EO}
S as sulfide [mass-%]	0.40	0.62	0.44	0.71	0.52	0.46	0.40	0.56	0.37	0.50	0.45

Pyrrhotite is below the limit of detection. Both samples contain thaumasite and calcite as products of cement paste alteration. In sample A1 gypsum is present as well. Portlandite is absent in both samples.

3.3. SEM/EDS

3.3.1. Aggregates

The same type of aggregates have been used in the construction of all four homes. The aggregates consist of phyllites and schists with quartz, albite, muscovite and chlorite as the main constituents. The phyllites exhibit a high content of sheet silicates and as a result, there is a high amount of "free" sheet silicate platelets embedded in the cement paste (Fig. 5). Muscovite and chlorite are present in a ratio of about 3:1. The length of the platelets as presented in the 2D view of the polished sections and thin section is typically <100 μm. Iron sulfides are mainly present as pyrrhotite ($Fe_{(1-X)}S$) with a smaller share of FeS_2: 87 % of the EDS point analysis performed on iron sulfides show pyrrhotite, while the rest is FeS_2 (210 points analyzed). As the amount of FeS_2 is too small to be detected in the XRD of the bulk sample, it is not clear, if FeS_2 is present as pyrite or marcasite. The majority of the analyzed pyrrhotite shows an atomic Fe/S-ratio > 0.92, indicating that monoclinic $Fe_{11}S_{12}$ is the dominant type of pyrrhotite [41]. The pyrrhotite is present in strongly varying degrees of oxidation. There is pyrrhotite with little traces of oxidation and pyrrhotite with more than half of the particle oxidized. In the majority of the cases, the oxidation does not progress from the surface towards the interior of the particles but develops as oxidation layers within the particle (Fig. 6). Additionally, there are traces of $CaCO_3$, phosphates, zircon, titanium oxide, pentlandite and chalcopyrite in the aggregates. In the oxidized layers present in pyrrhotite, the O/Fe-ratio of ~2 indicating that goethite (FeOOH) is more frequent than the Fe/O-ratio of ~3 indicating $Fe(OH)_3$. However, there are values in between 2 and 3 indicating a mixture of both phases. In some of these oxidized layers sulfur is present in concentrations up to 6 atom-%. This could indicate that some sulfur is present as water soluble sulfate in the oxidized layers.

3.3.2. Cement paste

Assessed qualitatively, the cement paste is very porous reflecting the high w/c and low strength of the concrete blocks. However, the degree of microcracking in the cement paste and debonding between aggregates is low. There are differences in the degree of carbonation between the different samples. The samples from homes A and E are mostly carbonated with only small parts showing remnants of uncarbonated cement hydrates. Sample D is carbonated to a lesser degree and sample P displays the highest amount of uncarbonated cement paste. However, the hydrates present in the uncarbonated parts of the samples are the same in all four cases. The same applies to the carbonated parts. As such the following information applies to all of them. Samples E from the inner leaf are completely carbonated.

The S/Ca- versus Al/Ca-ratio plot shows that portlandite (and possible some $CaCO_3$ as a first sign of carbonation), C-S-H, ettringite and thaumasite are present (Fig. 7). The S/Ca-ratio shows numerous points

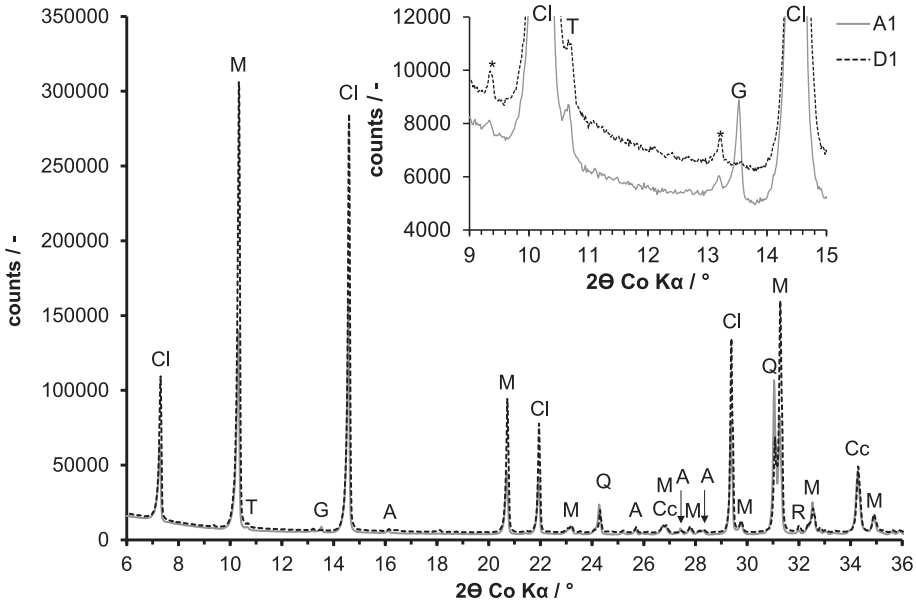

Fig. 4. XRD patterns of the fine fractions of samples A1 and D1. A = albite, CC = calcite, Cl = chlorite, G = gypsum, M = muscovite, Q = quartz, R = rutile, T = thaumasite, * = reflections not identified unambiguously. As further crystalline phase ankerite was identified (main reflection outside the displayed 2θ-range). The insert highlights the 2θ-region where the main reflections of thaumasite and gypsum occur.

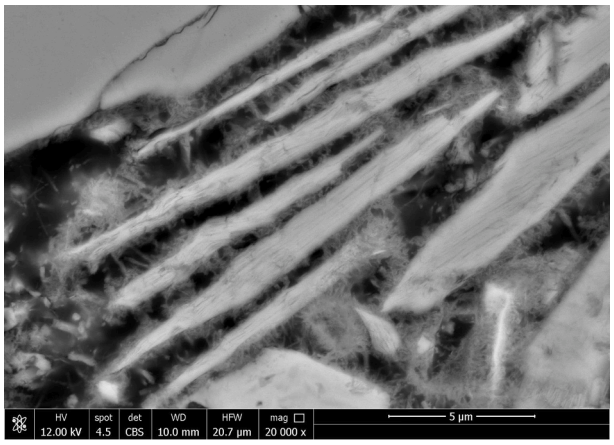

Fig. 5. Group of adjacent muscovite platelets with cement hydrates reinforcing the gaps between the platelets. Sample D.

that shift from thaumasite towards higher values. This indicates that finely distributed gypsum is present within these domains dominated by thaumasite. No monosulfate/monocarbonate is detectable. The shift in their direction (Fig. 7A) is caused by the presence of Si-Al-gel as clearly revealed in the Al/Ca- versus Si/Ca-ratio plot (Fig. 7B). Here, it can be seen that the Si/Ca-ratio of C-S-H is above its typical value in a PC systems (~ 0.54). This is caused by a partial de-calcification, either due to calcium consumption by thaumasite formation, by first signs of carbonation or a combination thereof. The Al/Ca-ratio of C-S-H clearly indicates that there is no problem in the analysis with an interference of small aggregate particles, as this would result in a considerably higher aluminum content of C-S-H. A typical situation for the four investigated samples is shown in Fig. 8. Monocarbonate is absent and there are pockets filled with ettringite. Furthermore, small sections of the cement paste are transformed to thaumasite. In extremes cases, entire sections of the cement paste are transformed to thaumasite (Fig. 9). Additionally, there are some pores with linings or complete fillings with ettringite and thaumasite (Fig. 10). Thaumasite is distributed inhomogeneously in the samples.

In the fully carbonated parts of the samples, the cement hydrate assemblage has been completely altered. The microstructure shows the typical features of carbonated cement paste, with dense clusters mainly formed by $CaCO_3$ and porous ones exhibiting low Ca content but high Si and Al content. The atomic ratio plots show that no ettringite or thaumasite is present anymore (Fig. 11A). C-S-H is partly de-calcified. Additionally, some C-S-H and the Al-containing phases ettringite and monocarbonate/monosulfate are transformed into an amorphous

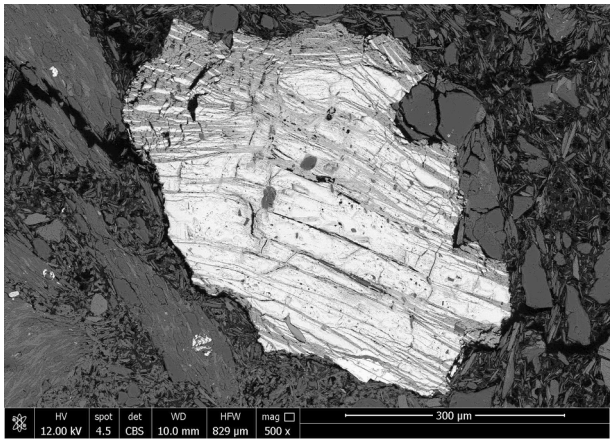

Fig. 6. Pyrrhotite particle in the cement paste showing layers of oxidation products (darker layers within the particle). Sample D.

product with an Al/Ca-ratio > 0.5 and a Si/Ca-ratio > 3 (Fig. 11B). Composition-wise, these products can be regarded as a precursor for zeolites. This phase and de-calcified C-S-H often contain a relatively high amount of magnesium that can be even higher than the one of calcium. Another product of carbonation, gypsum, is present either as relatively large particles in voids or in the cement paste (Fig. 12). Sometimes there are rims of $CaCO_3$ lining voids. Additionally, the S content of small clusters of $CaCO_3$ (diameter of 5–30 µm) formed by carbonation can reach values of up to 5 %. This indicates that small gypsum particles are embedded in such clusters.

The samples of the inner leaf show the same alteration of the cement paste as the carbonated areas from the outer leaf (Fig. 12). However, they do not exhibit the relatively large clusters of gypsum. Gypsum is still present but as more homogeneously distributed clusters with sizes in the micrometer range.

3.4. Thermodynamic modelling predictions

Thermodynamic modelling was used to investigate the potential changes occurring in hydrated PC and 10 g pyrrhotite per 100 g cement in the presence of oxygen and water and in the presence of CO_2 from the atmosphere.

In a first step, the effect of air (containing 21 % of O_2 and 0.042 % of CO_2) is calculated, whilst in a second step the effect of a complete carbonation is studied. The composition of the hydrated cements (without interaction with the environment) is shown on the left-hand

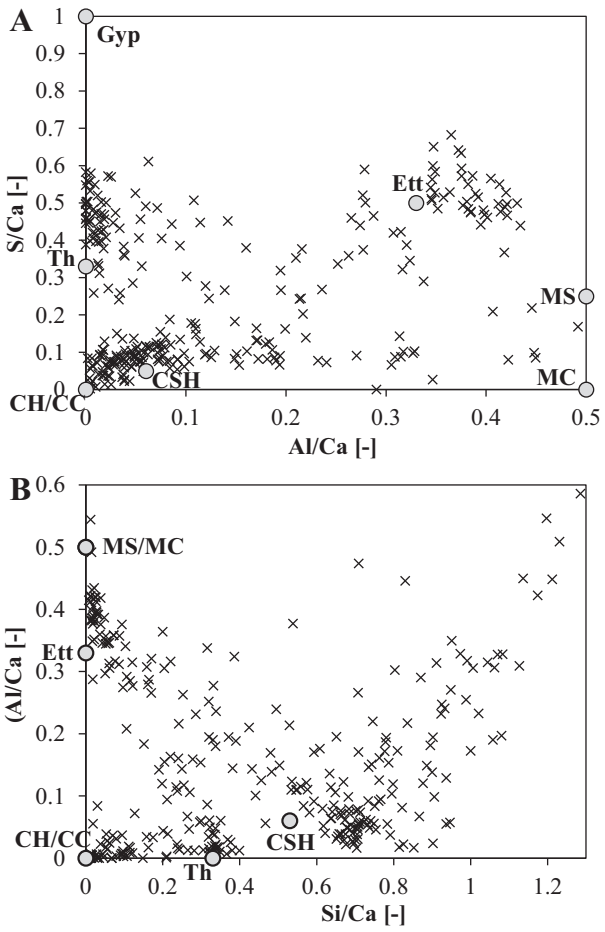

Fig. 7. S/Ca-ratio as a function of the Al/Ca-ratio (A) and Al/Ca-ratio as a function of the Si/Ca-ratio (B). The circles indicate the composition of different cement hydrates: CH = portlandite, CC = calcium carbonate, CSH = calcium-silicate-hydrate, MC = monocarbonate, MS = monosulfate, Th = thaumasite, Ett = ettringite, HG = hydrogarnet. Sample P. Number of points plotted: ~ 350.

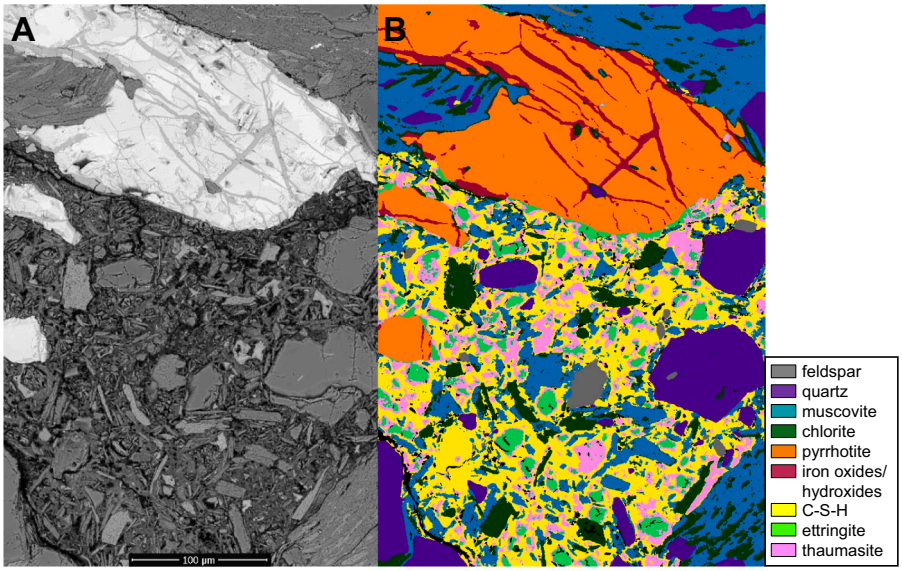

Fig. 8. Pyrrhotite in aggregate with oxidized layers and cement paste containing small clusters of both ettringite and thaumasite. Sample P.

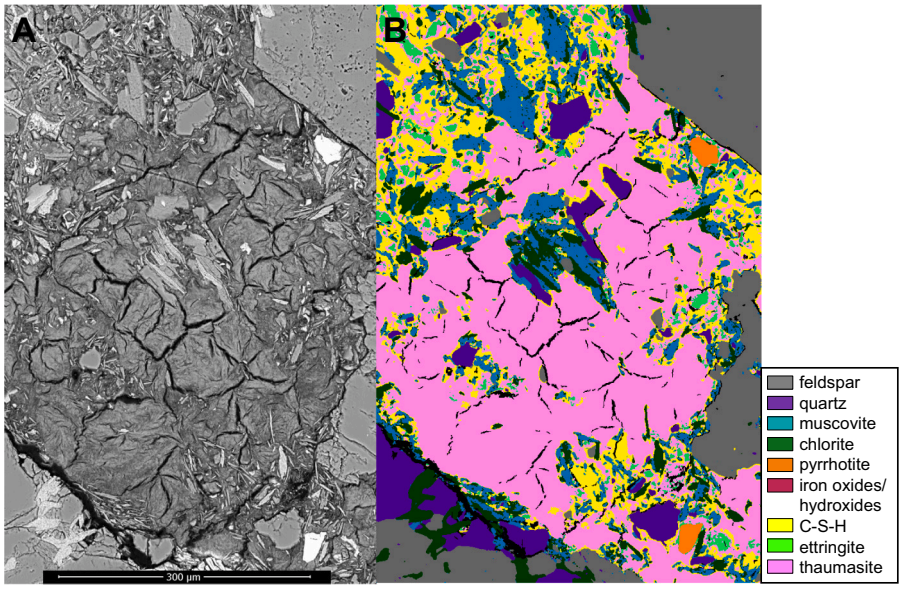

Fig. 9. Large cluster of thaumasite replacing the original cement paste. Sample P.

side of Fig. 13. A hydrate assemblage consisting of C-S-H, ettringite, portlandite, monocarbonate, and hydrotalcite was calculated, in agreement with the experimental observation reported in [38]. The Fe(III) originally present as Fe_2O_3 in the cement is in the presence of oxygen generally predicted and observed to precipitate as siliceous hydrogarnet: $Ca_3(Al,Fe)_2O_{7.66}Si_{0.84}(H_2O)_{4.32}$ [42,43]. In the presence of FeS, however, the formation of some magnetite, Fe_3O_4, is predicted based on the partial oxidation of sulfide, S(-II) to sulfate, ($S(VI)O_4^{2-}$), if water is available:

$$Fe_2O_3 + FeS + 5H_2O \geq Fe_3O_4 + SO_4^{2-} + 2H^+ + 4H_2 \quad (1)$$

Moving from left to right, Fig. 13 shows, the gradual changes towards the surface of the concrete exposed to the O_2 in the atmosphere, by increasing the amount of air in contact with the concrete. This allows to mimic the changes observed experimentally towards the surface of cement, mortar or concrete specimens as detailed e.g. in [28,29]. Such simplified thermodynamic models are very flexible and allow easy parameter variations and the results are in many cases comparable to full transport modelling, where parameters such as porosity and tortuosity have to be known in detail. A detailed comparison between the simplified modelling as used here and full transport modelling is given in [25,44].

The oxidation of FeS under reducing conditions (negative redox potential *pe*) leads to the formation of additional magnetite (Fe_3O_4) and ettringite, while monocarbonate and portlandite are consumed:

$$3FeS + Ca_4Al_2(CO_3)(OH)_{12}\cdot 5H_2O + 3Ca(OH)_2 + 18H_2O + 6.5O_2 \geq Fe_3O_4 + Ca_6Al_2(SO_4)_3(OH)_{12}\cdot 26H_2O + CaCO_3 \quad (2)$$

Once all FeS has been oxidized, the redox potential increases strongly, leading to the destabilization of the magnetite formed to Fe (III)-containing siliceous hydrogarnet ($Ca_3AlFeO_{7.66}Si_{0.84}(H_2O)_{4.32}$) and to a partial transformation of ettringite and C-S-H to thaumasite ($Ca_3(SiO_3)(SO_4)(CO_3)\cdot 15H_2O$):

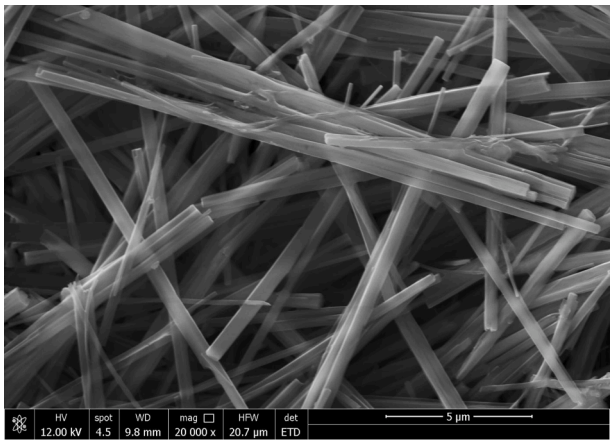

Fig. 10. SEM micrograph showing thaumasite present in the pores of sample P.

$$^{2}/_{3}Fe_3O_4 + Ca_6Al_2(SO_4)_3(OH)_{12}\cdot 26H_2O + 3CaCO_3 + 5Ca_{1.2}SiO_{3.2}\cdot 2H_2O + 11H_2O + 0.17O_2 => 2\ Ca_3AlFeO_8Si\cdot 4H_2O + 3Ca_3(SiO_3)(SO_4)(CO_3)\cdot 15H_2O \quad (3)$$

A simplified hydrogarnet ($Ca_3AlFeO_8Si\cdot 4H_2O$) and C-S-H ($Ca_{1.2}SiO_{3.2}\cdot 2H_2O$) composition was used to formulate reaction 3 to increase the readability, while in the thermodynamic calculations the correct formulas were used. Under oxic conditions, the formation of siliceous hydrogarnet (which contains Fe(III)) as well as the formation of thaumasite ($Ca_3(SiO_3)(SO_4)(CO_3)\cdot 15H_2O$) is predicted (see Fig. 13), in agreement with the EDS observations in Fig. 7. These oxidation reactions (Eqs. (2) and (3)) are associated with the binding of additional water in the solid phase and thus with a strong increase of the solid volume (20–25 %), which potentially could lead to cracking within the concrete structure comparable to observations during external sulfate attack [27,45].

The presence of the small fraction of CO_2 present in the air led to no significant carbonation during the calculations (Fig. 13), thus in a second step, the effect of additional carbonation (as expected upon long-term exposure to the air) was calculated by equilibrating hydrated cement to increasing amounts of CO_2 in the air as shown in Fig. 14. The modelling predicted the destabilization of portlandite, C-S-H, ettringite, thaumasite, hydrogarnet, and the formation of calcite, gypsum, Fe$(OH)_3$, traces of M-S-H, and zeolites (or SiO_2 and $Al(OH)_3$ if zeolite formation was suppressed in the calculations due to their slow formation kinetics). This results in moderate volume variations, comparable to the volume changes observed on PC without FeS upon carbonation as e.g. described in [28]. The volume increase at a pH of 13.5 after ettringite decomposition may indicate a potential for further damage.

If in the calculations first a complete carbonation is considered (which could occur if insufficient water is available for the oxidation reaction of pyrrhotite), this leads to the formation of calcite, gypsum and zeolites together with pyrrhotite and siderite ($FeCO_3$) as shown in Fig. 15. If oxidation would then occur in a completely carbonated PC, Fe$(OH)_3$ and additional gypsum are calculated to form from the oxidation of pyrrhotite and siderite. In both cases only moderate changes in the solid volume (<10 volume-%) occur.

In summary, thermodynamic modelling predicts a volume increase upon FeS oxidation of 22 volume-% due to the formation of additional ettringite, thaumasite and siliceous hydrogarnet, an additional increase of up to maximum 11 volume-% is calculated due to subsequent carbonation. In case complete carbonation would occur first, the calculated volume increase is much smaller (3 volume-% for carbonation and 8 volume-% for subsequent oxidation). If a cement containing siliceous mineral additions like fly ash was used, the amount of ettringite and thaumasite formed would be decreased due to the lower availability of calcium needed for their formation [46].

4. Discussion

4.1. Aggregates

Pyrrhotite in the aggregates used in the concrete blocks is partly oxidized. Oxidation can occur in the geological formation, in the stockpile after quarrying and after concrete production. It is not possible to attribute the amount of oxidation to each of these three different stages. However, the alteration of the cement hydrates is undeniable proof that at least part of the oxidation has taken place in the concrete. Pyrrhotite oxidation is connected to expansion that can lead to crack formation [3,15,16,78]. However, its expansion potential is regarded as significantly lower compared to the volume increase of the cement paste due to the sulfur release [3] as discussed in paragraph 5.2. Pyrrhotite oxidation shows both a dependence on relative humidity and pH. The oxidation rate increases significantly with increasing relative humidity [47] and is higher at pH 10 compared to pH 7 [48,49]. As such, a faster oxidation could be possible in the alkaline environment of uncarbonated concrete compared to the conditions in the geological formation, in the stockpile or in carbonated concrete.

The determined content of S present as sulfides in the concrete can be used to assess the iron sulfide content in the aggregates. When a bulk density of the concrete of 2050 kg/m^3 and an aggregate content of 1900 kg/m^3 are assumed, the mass percentages of sulfur present as sulfides

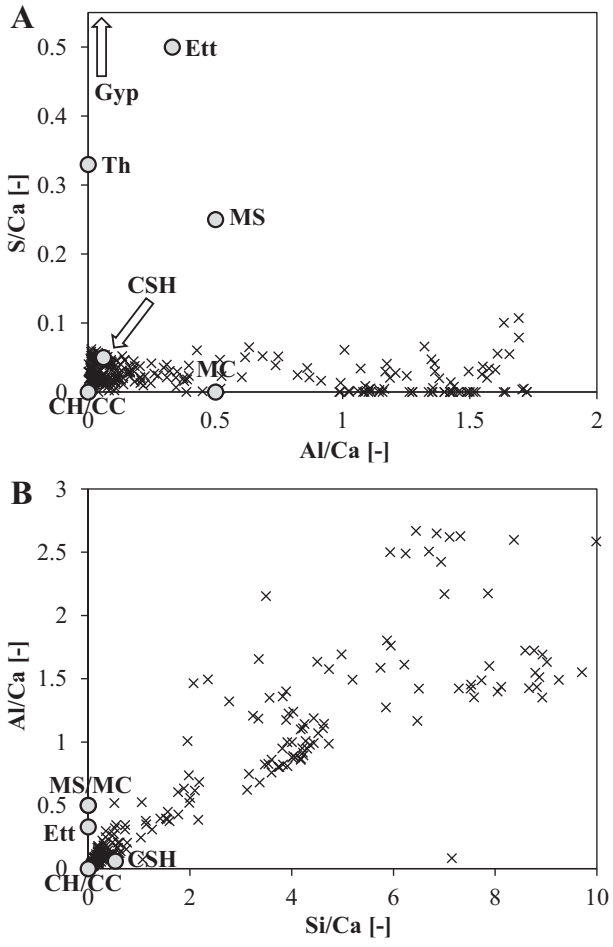

Fig. 11. S/Ca-ratio as a function of the Al/Ca-ratio (A) and Al/Ca-ratio as a function of the Si/Ca-ratio (B). For the labelling of the cement hydrates please refer to Fig. 6. Please note that gypsum having a S/Ca-ratio of 1 is out of the range shown in this plot. Carbonated locations of samples A2 and E.

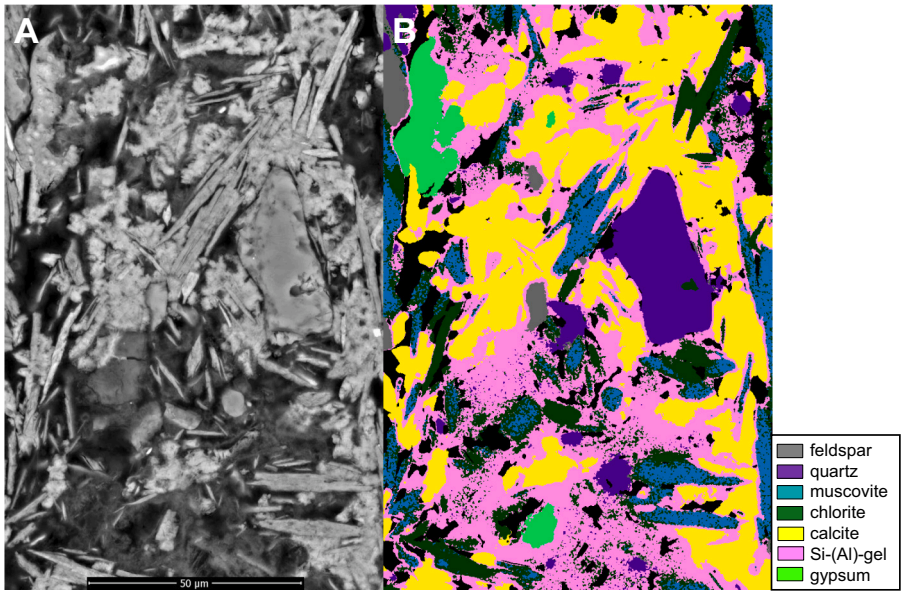

Fig. 12. BSE-image of the carbonated cement paste in sample A (left) and phase clustering of the same location (B) showing components of the aggregates and products of cement paste carbonation.

given in Table 2 can be multiplied by a factor of ~1.08 to reflect its content in the aggregates. This results in values between 0.43 and 0.77 mass-%, which is about 4 to 8 times higher than the value of 0.1 mass-% defined by the EN 12620 [39] as the limit for concrete aggregates containing pyrrhotite. With the assumed aggregate content of 1900 kg/m^3 and the results of EDS analysis, the content of iron sulfides can be calculated. This corresponds to 18–32 kg/m^3 of pyrrhotite and 3–5 kg/m^3 of FeS_2 comparing to 80–125 kg/m^3 of cement per m^3 of concrete (supplementary data, Table 1). The 74 homes in the data collection with appreciable amounts of pyrrhotite (supplementary data, Table 2) indicate that the situation there is comparable to the one of the four houses investigated in this study.

An increase of the original sulfur content of PC by a factor of 2–3 can already lead to substantial concrete expansion and considerable damage [50]. A typical SO_3 content in PC is ~3.5 mass-%. This is equal to a sulfur content of 1.5 kg/m^3 in a concrete block with cement content of 110 kg/m^3. In order to double this concentration, an amount of 4.4 kg/m^3 of pyrrhotite has to oxidize. Here, it has to be considered as well that an oxidizing pyrrhotite can be regarded as a point source of sulfur. Consequently, the sulfur level of the cement paste adjacent to an oxidizing pyrrhotite will be elevated above a factor of 2 even with a relative low oxidation level. As such, a concrete may expand due to ettringite formation in the cement paste surrounding an oxidizing pyrrhotite even if the total sulfur level of the concrete is not elevated considerably. These localized sulfate attacks are typical for oxidizing pyrrhotite [8,14,15].

Muscovite and chlorite are non-swellable sheet silicates [26]. Consequently, they do not exhibit a volume change upon contact with water and cannot cause stress in the concrete blocks as a result of changes in relative humidity. However, a high content of free sheet silicates influences the concrete properties [51,52]. It degrades workability of the fresh concrete due to the high specific surface area of the platelets and demands a higher water or cement paste content to reach a defined workability. Moreover, it may decrease compressive and flexural strength, if the concrete mix design is not adapted to their presence [51]. The effect of mica shows a strong dependence on grain size [51]. An addition of mica platelets corresponding to 2 mass-% of the aggregates with a size 500–1000 µm can lead to a decrease in compressive strength of ~20 %. If the same amount is added in a size <63 µm, the decrease is only in the range of 5 %. An amount of 2 mass-% of the aggregate corresponds to ~8 volume-% in the cement paste in the mix design chosen. This is slightly lower than the reported average of 9.4 volume-% (sum of muscovite and chlorite) in the Irish concrete blocks. Taking into account the slightly larger size of the mica platelets in the concrete blocks (< 100 µm) and their slightly higher amount, a less pronounced effect on concrete strength than the one mentioned above can be expected. While mica obviously affects compressive strength, the resistance to frost seems to be impacted considerably less [53]. In any case, I.S.465 clearly states in regard to the impact of mica on workability and strength that "these disadvantageous effects of mica can be adequately compensated by slightly increasing the contents of cement in the mix design or by using an admixture" [2]. Moreover, the required characteristic compressive strength of the concrete blocks is 7.5 MPa independent of their mica content. As such, the presence of mica in the concrete blocks should not be of concern in regard to compressive strength.

4.2. Alteration of the cement paste

The microstructural analysis shows that two different decoupled processes lead to an alteration of the cement hydrates. One is internal sulfate attack triggered by iron sulfide oxidation, the other one is carbonation.

The oxidation of iron sulfides leads to the release of sulfur, likely in the form of sulfuric acid (H_2SO_4). As the pore solution of concrete is highly alkaline (pH 13.0–13.5), the protons can be expected to be buffered immediately. As a result, there is no precipitation of gypsum and sulfate remains in the pore solution of the concrete. Here, it can react with monosulfate/monocarbonate to form secondary ettringite, leading to expansion and eventually cracking [6,54,55]. Once monosulfate/monocarbonate has reacted, thaumasite can form as observed in the samples (EDS and XRD analysis) and confirmed by thermodynamic modelling (Fig. 13). Thaumasite needs a source of carbonates in order to form [56]. The minor amounts of $CaCO_3$ present in the aggregates, in limestone filler used as a minor component in the PC or CO_2 chemically bound by cement hydrates can provide such a source. Thaumasite formation can lead to a significant strength decrease of the concrete as it consumes C-S-H and portlandite [47,57,58] and may degrade the concrete to a soft mush in extreme cases [59]. The kinetics of thaumasite formation show a dependence on temperature: they increase with

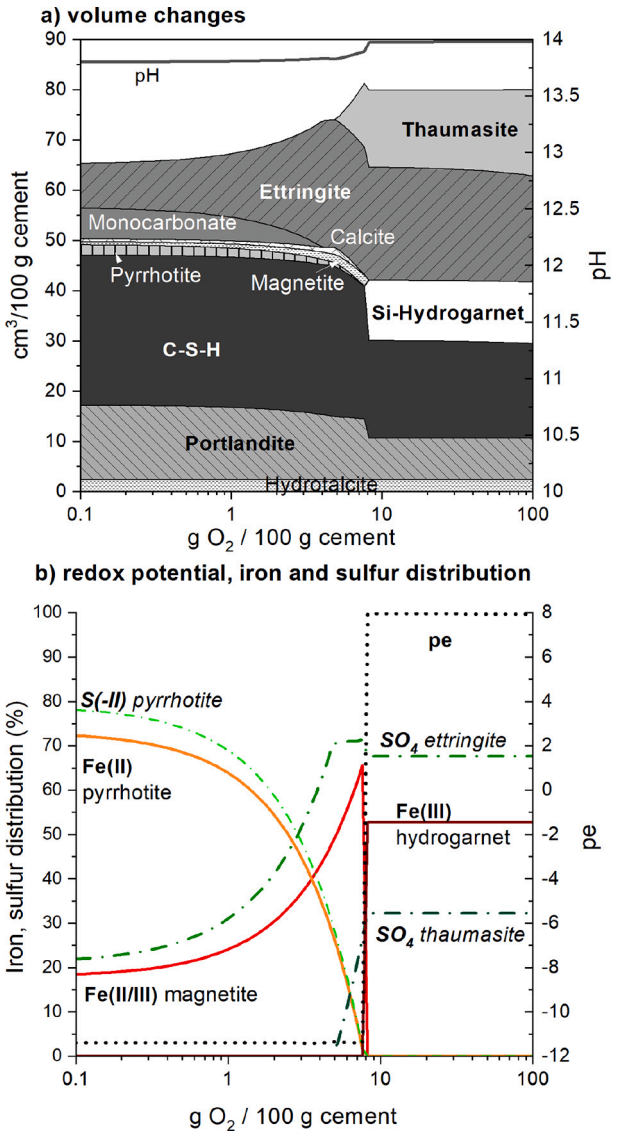

Fig. 13. Predicted a) volume of phases and pH values, b) redox potential and iron and sulfur distribution in the solid phases of a hydrated Portland concrete containing 10 g FeS per 100 g unhydrated cement (w/c of 0.60) exposed to increasing amounts of air at 10 °C. The aggregates with exception of pyrrhotite (FeS) are assumed to be inert and are not shown. The phases are given in [cm^3/100 g cement] based on the PC composition from [38]. FeS: pyrrhotite; C-S-H: calcium-silicate-hydrate. Redox potential (pe = −log(activity of e-); negative *pe* values indicate reducing conditions, positive oxidizing conditions), Fe(II), Fe (III), S(-II) and S(VI) distribution as mol-% in the solid phase.

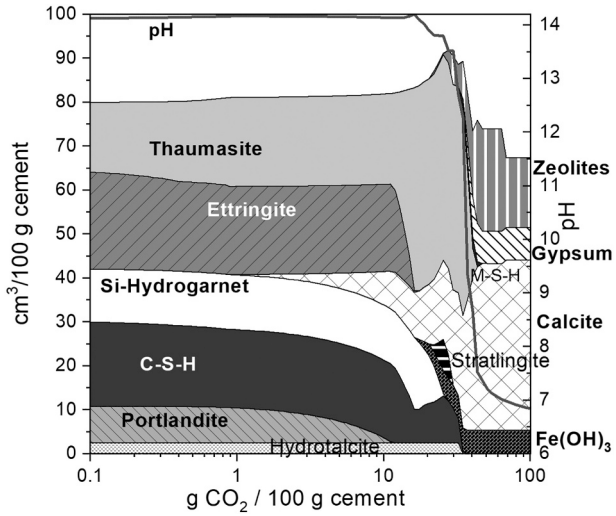

Fig. 14. Predicted pH values and volume in the solid phases of a hydrated and oxidized Portland concrete containing 10 g FeS per 100 g unhydrated cement exposed to increasing amounts of CO_2 in the air at 10 °C. The phases are given in [cm^3/100 g cement] based on the PC composition from [38].

decreasing temperature [56,57,60,61]. However, thaumasite can form in cementitious systems at a temperature as high as 20 °C [62–64]. Once formed, thaumasite is stable at temperatures well above 20 °C [65]. As such, the temperatures in Donegal with monthly means between 5 and 15 °C [66] provide favorable conditions for thaumasite to form. The shift in the atomic-ratio plots from thaumasite towards gypsum (Fig. 7) at an advanced state of the reaction indicates that locally very high levels of sulfur are reached in the cement paste. The inhomogeneous distribution of thaumasite is likely linked to the inhomogeneous distribution of oxidizing pyrrhotite leading to very high sulfur contents locally.

Carbonation can affect this reaction on different levels. The reservoir of $CaCO_3$ supporting thaumasite formation is increased at an early stage of carbonation [67]. Additionally, it leads to a decreasing pH in the concrete. This triggers an increased kinetics of thaumasite formation [68]. With an increasing level of carbonation, portlandite is completely altered to $CaCO_3$ and C-S-H is decalcified. When the pH decreases below 10, ettringite and thaumasite are not stable anymore [28,69] and decompose. The resulting phases are shown by the atomic-ratio plots (Fig. 11), the phase clustering (Fig. 12) and the thermodynamic modelling (Fig. 14): $CaCO_3$, decalcified C-S-H, Si-Al-gel with a composition similar to zeolites, and gypsum (Fig. 11). The XRD analysis shows the presence of gypsum only in sample A1 (Fig. 4). As the location from which sample D1 was taken, was exposed to direct rain, gypsum was likely dissolved and washed out before sampling. The relatively high concentration of magnesium in de-calcified C-S-H and the Si-Al-gel can be attributed to the partial dissolution of chlorite in the cementitious system as confirmed by the thermodynamic data [36]. The occasionally occurring rims of $CaCO_3$ at the edge of voids indicate partial dissolution and re-precipitation. The relatively large clusters of gypsum, in particular the ones forming in voids, indicate dissolution of small particles and re-precipitation as larger ones as well. This is likely linked to weather-induced changes in the moisture content of the concrete blocks in the outer leaf. As such, changes are not present in the inner leaf, large clusters of gypsum are not present there. Still, even the small clusters are not typical for a carbonated concrete, indicating an increased sulfur content in the cement paste.

The higher the degree of carbonation at the time of internal sulfate attack, the lower is the potential for ettringite and thaumasite formation. In the extreme case of complete carbonation of the cement hydrates at the time of sulfur release by pyrrhotite oxidation, only gypsum will form as new sulfur-containing phase (Fig. 15). In this case, it can be expected the sulfuric acid generated by pyrrhotite oxidation dissolves calcium from the cement paste and causes gypsum to precipitate. As the precipitation occurs mainly in existing voids no substantial concrete expansion is to be expected as it is indicated as well by thermodynamic modelling (Fig. 15). As calcium is dissolved from the carbonated cement paste, a certain strength loss is still possible. However, the significant expansion and cracking in the outer leaf walls clearly indicate a substantial internal sulfate attack before carbonation is able to decrease the damage potential.

The boundary conditions for internal sulfate attack and carbonation differ in the outer and inner leaf of the homes. Whereas carbonation progresses the fastest at a relative humidity of about 60 % [70,71], pyrrhotite oxidation increases significantly with increasing relative humidity [47]. Therefore, it can be expected that internal sulfate attack proceeds faster in the outer compared to the inner leaf. Carbonation on

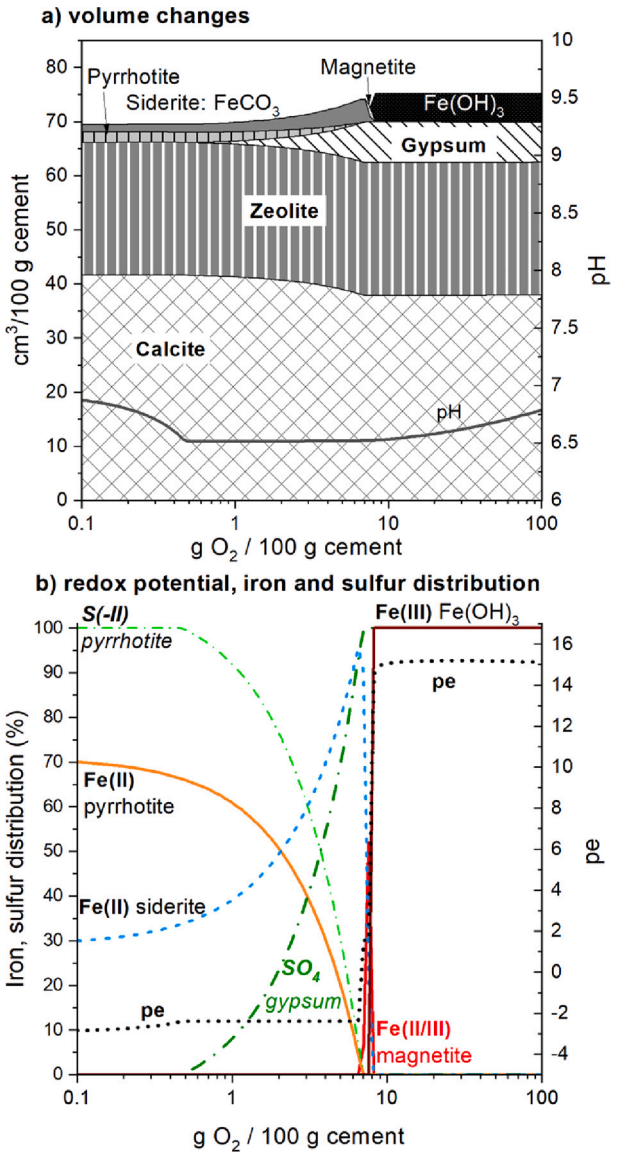

Fig. 15. Predicted a) volume of phases and pH values, b) redox potential and iron and sulfur distribution in the solid phases of a completely carbonated Portland cement concrete containing 10 g FeS per 100 g unhydrated cement exposed to increasing amounts of air at 10 °C. The aggregates with exception of pyrrhotite (FeS) are assumed to be inert and are not shown. The phases are given in [cm^3/100 g cement] based on the PC composition from [38]. FeS: pyrrhotite; C-S-H: calcium-silicate-hydrate. Redox potential (pe = −log(activity of e-); negative *pe* values indicate reducing conditions, positive oxidizing conditions), Fe(II), Fe(III), S(-II) and S(VI) distribution as mol-% in the solid phase.

the other hand progresses faster in the inner leaf. As such, the potential for damage is higher in the outer compared to the inner leaf. This situation is evident from the investigated homes and from the data collection (supplementary data, Table 2). Although cracks are less frequent in the inner compared to the outer leaf, they can still be observed in numerous homes (supplementary data, Table 2). Although pyrrhotite oxidation is slower and carbonation is faster in the inner leaf, internal sulfate attack in the inner leaf cannot be excluded. This is indicated as well by the formation of gypsum in the inner leaf of home E. Furthermore, it can be expected that concrete quality has an effect on the interrelation between internal sulfate attack and carbonation. Moisture available for iron sulfide oxidation in a higher quality concrete than present in the blocks may not be decreased significantly, as water vapor diffusion and capillary suction [72,73] from the surface of the blocks in contact with the render will still enable transport. On the other hand, carbonation kinetics decreases significantly with increasing concrete quality, in particular at a relative humidity >70 % [70,74]. As such, the probability for a reduced extent of internal sulfate attack by carbonation may be lower in the case of a higher quality concrete.

Formation of cracks perpendicular to the surface of the outer leaf may influence internal sulfate attack. It has been observed in the outer leaf that once cracks have formed, the progress of deterioration seems to accelerate as indicated by the relatively fast widening of the cracks. This could be related to an easier availability of moisture boosting internal sulfate attack once the shielding effect of the plaster is decreased.

4.3. Probability of frost attack

It is stated in I.S.465 that "excessive quantities of free muscovite mica in aggregate can render the blocks susceptible to freeze thaw degradation when saturated" [2]. Sub-zero temperatures can occur in Donegal, but they are uncommon due to the Atlantic influence on Ireland's climate. In the previous two decades, only two prolonged cold periods have occurred where below freezing temperatures were experienced in many areas across Ireland. The first was in mid December 2009 to early January 2010, when the mean air temperatures were around two degrees lower than average for the 1961–90 period. It was the coldest winter since 1962/3. The lowest temperatures measured were on December 24th to 25th and 7th to 9th January, when air temperatures dropped below −10 °C in places (Met Eireann). A similar cold event happened after the middle of November 2010. Met Eireann, the Irish National Meteorological Service, estimates a return period of approximately 1 in 25–30 years for such events [75]. These temperatures however are far from the norm and average temperatures in Donegal are typically well above these extreme events, with only a few days experiencing zero to subzero temperatures annually. The Inishowen Peninsula in North Donegal is considered the epicenter of the defective block crisis and has the highest concentration of affected homes and other buildings numbering in the thousands. Malin Head, Ireland's most northerly point, is at the northern tip of the peninsula. Climate records from Malin Head meteorological station, available from Met Eireann's online portal, show that only 50 days with zero or sub zero temperature were recorded there during the last 10 years (Fig. 16). Only three other meteorological stations with long term daily temperature

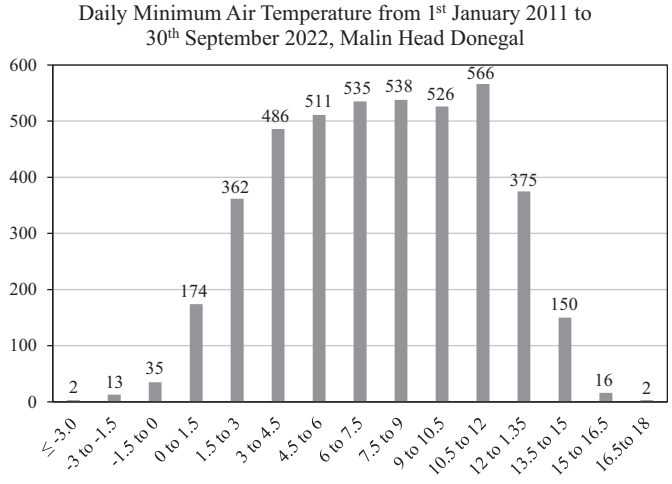

Fig. 16. Histogram of all the daily minimum temperature readings recorded at Malin Head weather station, Donegal from January 2011 to September 2022. This is Ireland's most northerly point and from a total of 4291 days, only 50 were 0 °C or below (This data is published under a Creative Commons Attribution 4.0 International (CC BY 4.0). To view a copy of this license, visit https://creativecommons.org/licenses/by/4.0/. Source: www.met.ie, copyright Met Éireann [75]).

records are available for Donegal on this portal. These are Glenties, Finner and Ballyshannon and all have recorded more days with frost than occurred at Malin Head for the previous 10 years. However, these stations are situated over 100 km southwest of the center of Inishowen, and to date there have been very few reports of affected homes in southwest Donegal in the vicinity of these three stations. Temperatures as recorded at Malin Head cannot lead to frost damage of the concrete blocks. As the blocks are protected by a 2–3 cm thick layer of plaster they are hardly exposed to frost, when the temperature decreases to a few degrees below zero during the night and reaches temperatures above zero during the day. Within these boundary conditions temperature in concrete is a few degrees higher in a depth $\geq$ 25 mm compared to the concrete surface [76,77]. Moreover, a high degree of water saturation as a prerequisite for frost damage is usually not reached on vertical surfaces like walls. When a concrete is not saturated, freezing temperature of water decreases with decreasing saturation degree. As an example, water in a concrete with a water-to-cement ration of 0.63 freezes at about −10 and −20 °C at relative internal humidity values of 94 and 90 %, respectively [78]. The damage characteristics are another strong indication against frost as the mechanism. Frost damage on the walls would be expected to manifest as surface parallel cracking and scaling, decreasing in severity with increasing distance from the surface exposed to the environment. This is in pronounced contrast to the cracking and damage observed in affected homes in Donegal. Cracks form perpendicular to the surface of the walls and often extend from the ground up to the roof. Some of them even propagate from the roof down, far above the typical frost zone at ground level. The purported frost damage is in contrast as well to the strength loss and crumbling of the concrete affecting the entire cross-section of the blocks to the same degree. Moreover, it has to be pointed out that the deterioration of the homes has progressed significantly after the last extreme frost event in 2009/10. In addition, there are homes that started to crack before 2009/2010 [1] and three houses in the data collection (supplementary data) exhibiting the typical damage were built after the 2009/10 frost events. As such, frost as a main cause for the observed damage can be excluded, while it can be at best a secondary contributing factor after the initial cracking due to internal sulfate attack has occurred. Even if this type of concrete is unlikely to be frost resistant in a typical accelerated test that includes multiple frost cycles down to temperatures in the range of −20 °C of completely water saturated samples [79,80], such conditions are not comparable to the ones in the outer leaf of Donegal homes and are therefore not transferable.

5. Conclusions

A detailed analysis of the microstructure of concrete cores from four damaged homes in county Donegal was performed. Additionally, the content of sulfur in the concrete present as sulfide was determined. Thermodynamic modelling allowed the display of the changes in the assemblage of the cement hydrates supporting the microstructural analysis in a novel combination of these two techniques in regard to internal sulfate attack. The data collection of 91 homes in Donegal enabled the assessment of the representativeness of the obtained results.

The damage observed in the four investigated homes point to internal sulfate attack triggered by pyrrhotite oxidation with the release of sulfur:

- Phase 1: The sulfur release leads to the transformation of monosulfate/monocarbonate to ettringite accompanied by concrete expansion.
- Phase 2: Further release of sulfur leads to the formation of thaumasite and eventually gypsum accompanied by a strength decrease of the concrete

Simultaneously to internal sulfate attack, concrete carbonation takes place with both reactions influenced by relative humidity in an opposite way. Kinetics of pyrrhotite oxidation increase and kinetics of carbonation decrease with increasing relative humidity. The opposite situation applies with decreasing relative humidity. This interrelation affects internal sulfate attack in several ways:

- The increasing availability of carbonates and the decrease of pH caused by carbonation boost thaumasite formation and strength loss during simultaneous or preceding internal sulfate attack.
- In the case of complete carbonation after internal sulfate attack, gypsum remains the only sulfate mineral. It is the only mineralogical indication left that phases 1 and 2 have taken place.
- The higher the degree of carbonation at the time of sulfur release by pyrrhotite oxidation, the lower is the amount of ettringite and thaumasite formed and the potential for damage.
- In the case of complete concrete carbonation, it can be expected that calcium is dissolved by sulfuric acid and gypsum precipitates in existing voids without leading to substantial concrete expansion during internal sulfate attack. It may still lead to a certain strength decrease due to the calcium dissolution.
- Due to the reasons stated above, the potential for concrete damage is higher in the outer leaf compared to the drier inner leaf.

The expansion caused by the formation of iron oxides and hydroxides going along with iron sulfide oxidation is superimposed onto the effects of cement paste alteration by released sulfur. As such, it takes place independently of the type of sulfate minerals formed and carbonation.

The majority of homes in the data collection contain appreciable amounts of pyrrhotite matching the diagnosis of the four investigated homes. Consequently, it is highly likely that the damage observed in the homes of the data collection are as well caused by internal sulfate attack. Therefore, the results of this study can be regarded as representative for the mechanism of damage occurring in the so-called “Mica crisis” affecting thousands of homes in Donegal.

Frost as the cause for the damage in the investigated homes can be excluded due to the boundary conditions in regard to temperature and the characteristics of damage. After initial cracking due to internal sulfate attack has occurred, it may be a contributing factor at best.

6. Outlook

An in-depth analysis of the cement hydrates in additional homes has to be performed and the data collection has to be expanded. In particular, more samples from homes where the inner leaf exhibits cracks have to be studied in order to assess the inherent damage potential. Moreover, the concrete foundations of the homes have to be included in the microstructural analysis as they have the potential to be affected by internal sulfate attack when they contain aggregates with appreciable amounts of pyrrhotite. The use of wavelength dispersive X-Ray analysis should be used to further characterize the iron sulfides present in the aggregates. Additionally, micro-X-ray fluorescence may provide further information on the sulfur distribution in the concrete on a millimeter to centimeter scale.

CRediT authorship contribution statement

Andreas Leemann: Conceptualization, Methodology, Validation, Investigation, Formal analysis, Data curation, Writing – original draft, Writing – review & editing, Visualization, Project administration. **Barbara Lothenbach:** Conceptualization, Methodology, Validation, Formal analysis, Writing – original draft, Writing – review & editing, Visualization. **Beat Münch:** Formal analysis, Writing – review & editing. **Thomas Campbell:** Resources, Writing – review & editing. **Paul Dunlop:** Conceptualization, Methodology, Investigation, Writing – original draft, Writing – review & editing, Project administration.

Declaration of competing interest

Based on the collaboration with Ulster University on the topic of concrete durability related to the "Mica crisis", Andreas Leemann was awarded the honorary title of Visiting Professor attached to the School of Geography and Environmental Sciences at Ulster University (UK) from 31 August 2022 to 30 April 2026. He receives no salary in connection with this position.

Paul Dunlop is an affected home owner and following I.S. 465 protocols his home has been approved for demolition as part of the Irish Government's Defective Concrete Blocks Grant Scheme.

Apart from sampling and shipping costs that were funded by the School of Geography and Environmental Sciences at Ulster University, the research presented in this paper did not receive any funding.

Data availability

Data will be made available on request.

Acknowledgements

The authors would like to thank the owners of the four investigated homes for permitting the extraction of cores and providing the test reports. Frank Winnefeld is acknowledged for the XRD analysis and Pietro Lura for reviewing the manuscript. Additionally, the authors would like to thank the two anonymous peer reviewers for their work.

Appendix A. Supplementary data

Supplementary data to this article can be found online at https://doi.org/10.1016/j.cemconres.2023.107149.

References

[1] D. McCarthy, N. Kane, F. Lee, D. Blaney, Report of the Expert Panel on Concrete Blocks, Department of Housing, Local Government and Heritage, 2017. https://www.gov.ie/en/publication/0218f-report-of-the-expert-panel-on-concrete-blocks/.
[2] National Standards Authority of Ireland, I.S. 465:2018+A1:2020, Assessment, Testing and Categorisation of Damaged Buildings Incorporating Concrete Blocks Containing Certain Deleterious Materials and Amendment 1, 2020.
[3] I. Casanova, L. Agulló, A. Aguado, Aggregate expansivity due to sulfide oxidation - I. Reaction system and rate model, Cem. Concr. Res. 26 (7) (1996) 993–998.
[4] H. Lee, R.D. Cody, A.M. Cody, P.G. Spry, The formation and role of ettringite in Iowa highway concrete deterioration, Cem. Concr. Res. 35 (2) (2005) 332–343.
[5] T. Schmidt, A. Leemann, E. Gallucci, K. Scrivener, Physical and microstructural aspects of iron sulfide degradation in concrete, Cem. Concr. Res. 41 (3) (2011) 263–269.
[6] I. Oliveira, S.H. Cavalaro, A. Aguado, New kinetic model to quantify the internal sulfate attack in concrete, Cem. Concr. Res. 43 (2013) 95–104.
[7] X. Han, C. Pang, R. Gao, S. Wu, W. Sun, Iron sulfide-related internal sulfate attack: microstructure and mechanism, Mag. Concr. Res. 70 (8) (2018) 379–389.
[8] A. Rodrigues, J. Duchesne, B. Fournier, B. Durand, P. Rivard, M. Shehata, Mineralogical and chemical assessment of concrete damaged by the oxidation of sulfide-bearing aggregates: importance of thaumasite formation on reaction mechanisms, Cem. Concr. Res. 42 (10) (2012) 1336–1347.
[9] A. Rodrigues, J. Duchesne, B. Fournier, A new accelerated mortar bar test to assess the potential deleterious effect of sulfide-bearing aggregate in concrete, Cem. Concr. Res. 73 (2015) 96–110.
[10] J. Francoeur, Étude de l'évolution de la deterioration du béton incorporant des granulats riches en sulfures de fer, Université Laval (Québec, Canada), 2016. MSc thesis.
[11] A. Rodrigues, J. Duchesne, B. Fournier, B. Durand, M. Shehata, P. Rivard, Evaluation protocol for concrete aggregates containing iron sulfide minerals, ACI Mater. J. 113 (3) (2016) 349–359.
[12] A. Rodrigues, J. Duchesne, B. Fournier, Quantitative assessment of the oxidation potential of sulfide-bearing aggregates in concrete using an oxygen consumption test, Cem. Concr. Compos. 67 (2016) 93–100.
[13] L.F.M. Sanchez, T. Drimalas, B. Fournier, Assessing condition of concrete affected by internal swelling reactions (ISR) through the Damage Rating Index (DRI), Cement (2020), https://doi.org/10.1016/j.cement.2020.100001.
[14] R. Zhong, K. Wille, Deterioration of residential concrete foundations: the role of pyrrhotite-bearing aggregate, Cem. Concr. Compos. 94 (2018) 53–61.
[15] D. Jana, Pyrrhotite epidemic in eastern Connecticut: diagnosis and prevention, ACI Mater. J. 117 (1) (2020).
[16] D. Jana, Cracking of residential concrete foundations in eastern Connecticut, USA from oxidation of pyrrhotite, Case Stud.Constr. Mater. 16 (2022), e00909.
[17] EN 771-3:2011+A1, Specification for Masonry Units - Part 3: Aggregate Concrete Masonry Units (Dense and Lightweight Aggregates), 2015.
[18] Irish Concrete Federation, Guide for Specifiers and Manufacturers on I.S. EN 771-3: Aggregate Concrete Masonry Units, 2018. Dublin.
[19] DIN EN 196-2:2013-10: Method of testing cement - Part 2: Chemical analysis of cement; German version.
[20] BS EN 1744-1:2009+A1, Tests for Chemical Properties of Aggregates Chemical Analysis, 2012.
[21] K. Scrivener, A.B. Bazzoni, J.E.Rossen Mota, Electron microscopy, in: K. Scrivener, R. Snellings, B. Lothenbach (Eds.), A Practical Guide to Microstructural Analysis of Cementitious Materials, CRC Press, Boca Raton (FL, USA), London (UK) and New York (NY, USA), 2016, pp. 352–417.
[22] B. Münch, L.H. Martin, A. Leemann, Segmentation of elemental EDS maps by means of multiple clustering combined with phase identification, J. Microsc. 260 (3) (2015) 411–426.
[23] E. Pavón, M.D. Alba, Swelling layered minerals applications: a solid state NMR overview, Prog. Nucl. Mag. Res. SP. 124 (2021) 99–128.
[24] R. Loser, B. Lothenbach, A. Leemann, M. Tuchschmid, Chloride resistance of concrete and its binding capacity – comparison between experimental results and thermodynamic modeling, Cem. Concr. Compos. 32 (1) (2010) 34–42.
[25] B. Lothenbach, B. Bary, P. Le Bescop, T. Schmidt, N. Leterrier, Sulfate ingress in Portland cement, Cem. Concr. Res. 40 (8) (2010) 1211–1225.
[26] A. Leemann, B. Lothenbach, H. Siegrist, C. Hoffmann, Influence of water hardness on concrete surface deterioration caused by nitrifying biofilms in wastewater treatment plants, Int. Biodeterior. Biodegradation 64 (6) (2010) 489–498.
[27] W. Kunther, B. Lothenbach, K. Scrivener, On the relevance of volume increase for the length changes of mortar bars in sulfate solutions, Cem. Concr. Res. 46 (2013) 23–29.
[28] Z. Shi, B. Lothenbach, M.R. Geiker, J. Kaufmann, A. Leemann, S. Ferreiro, J. Skibsted, Experimental studies and thermodynamic modeling of the carbonation of Portland cement, metakaolin and limestone mortars, Cem. Concr. Res. 88 (2016) 60–72.
[29] C.W. Hargis, B. Lothenbach, C.J. Müller, F. Winnefeld, Carbonation of calcium sulfoaluminate mortars, Cem. Concr. Compos. 80 (2017) 123–134.
[30] D. Kulik, T. Wagner, S. Dmytrieva, G. Kosakowski, F. Hingerl, K. Chudnenko, U. Berner, GEM-selektor geochemical modeling package: revised algorithm and GEMS3K numerical kernel for coupled simulation codes, Computat. Geosci. 17 (1) (2013) 1–24.
[31] T. Thoenen, W. Hummel, U. Berner, E. Curti, The PSI/Nagra Chemical Thermodynamic Database 12/07, PSI Report 14-04, Villigen PSI, Switzerland, 2014.
[32] B. Lothenbach, D.A. Kulik, T. Matschei, M. Balonis, L. Baquerizo, B. Dilnesa, G. D. Miron, R.J. Myers, Cemdata18: a chemical thermodynamic database for hydrated Portland cements and alkali-activated materials, Cem. Concr. Res. 115 (2019) 472–506.
[33] B. Ma, B. Lothenbach, Synthesis, characterization, and thermodynamic study of selected Na-based zeolite, Cem. Concr. Res. 135 (2020), 106111.
[34] B. Ma, B. Lothenbach, Thermodynamic study of cement/rock interactions using experimentally generated solubility data of zeolites, Cem. Concr. Res. 135 (2020), 106149.
[35] B. Ma, B. Lothenbach, Synthesis, characterization, and thermodynamic study of selected K-based zeolites, Cem. Concr. Res. 148 (2021), 106537.
[36] H.C. Helgeson, Summary and critique of the thermodynamic properties of rock-forming minerals, Am. J. Sci. 278 (1978) 1–229.
[37] D.A. Kulik, Improving the structural consistency of C-S-H solid solution thermodynamic models, Cem. Concr. Res. 41 (5) (2011) 477–495.
[38] B. Lothenbach, G. Le Saout, E. Gallucci, K. Scrivener, Influence of limestone on the hydration of Portland cements, Cem. Concr. Res. 38 (6) (2008) 848–860.
[39] EN 12620, Aggregates for Concrete, 2013.
[40] National Standards Authority of Ireland, Guidance on the Use of I.S. EN 12620: 2002+A1:2008 – Aggregates for Concrete, 2016.
[41] J. Duchesne, A. Rodrigues, B. Fournier, Concrete damage due to oxidation of pyrrhotite-bearing aggregate: a review, RILEM Tech. Lett. 6 (2021) 82–92.
[42] B.Z. Dilnesa, B. Lothenbach, G.Le Saout, E. Wieland, K.L. Scrivener, Fe-containing Hydrates in Cementitious Systems. ICCC 2011, Madrid, 2011.
[43] M. Vespa, E. Wieland, R. Dähn, B. Lothenbach, Identification of the thermodynamically stable Fe-containing phase in aged cement pastes, J. Am. Ceram. Soc. 98 (7) (2015) 2286–2294.
[44] K. De Weerdt, E. Bernard, W. Kunther, M.T. Pedersen, B. Lothenbach, Phase changes in cementitious materials exposed to saline solutions, Cem. Concr. Res. 165 (2023), 107071.
[45] A. Leemann, R. Loser, Analysis of concrete in a vertical ventilation shaft exposed to sulfate-containing groundwater for 45 years, Cem. Concr. Compos. 33 (1) (2011) 74–83.
[46] F. Bellmann, J. Stark, The role of calcium hydroxide in the formation of thaumasite, Cem. Concr. Res. 38 (10) (2008) 1154–1161.
[47] H.F. Steger, Oxidation of sulfide minerals: VII. Effect of temperature and relative humidity on the oxidation of pyrrhotite, Chem. Geol. 35 (3–4) (1982) 281–295.
[48] Z. Ekmekci, M. Becker, E.B. Tekes, D. Bradshaw, The relationship between the electrochemical, mineralogical and flotation characteristics of pyrrhotite samples from different Ni ores, J. Electroanal. Chem. 647 (2010) 133–143.
[49] M. Becker, J. de Villiers, D. Bradshaw, The flotation of magnetic and nonmagnetic pyrrhotite from selected nickel ore deposits, Miner. Eng. 23 (2010) 1045–1052.

[50] R. Loser, A. Leemann, An accelerated sulfate resistance test for concrete, Mater. Struct. 49 (8) (2016) 3445–3457.
[51] A. Leemann, L. Holzer, Influence of mica on the properties of mortar and concrete, in: Proceedings of the 8th Euroseminar on Microscopy Applied to Buildings Materials. Athens/Greece, 2001, pp. 199–204.
[52] G.R. Maregesi, Mica in concrete, Adv. Eng. Sol. J. 1 (2021) 1–7.
[53] J.Q. Xing, S.L. Zhan, X.Y. Li, Effect of mica content in stone powder of manufactured sand on performance of cement mortar, Adv. Mater. Res. 1044 (2014) 624–628.
[54] T. Schmidt, B. Lothenbach, M. Romer, J. Neuenschwander, K. Scrivener, Physical and microstructural aspects of sulfate attack on ordinary and limestone blended Portland cements, Cem. Concr. Res. 39 (12) (2009) 1111–1121.
[55] W. Kunther, B. Lothenbach, J. Skibsted, Influence of the Ca/Si ratio of the C-S-H phase on the interaction with sulfate ions and its impact on the ettringite crystallization pressure, Cem. Concr. Res. 69 (2015) 37–49.
[56] T. Schmidt, B. Lothenbach, M. Romer, K. Scrivener, D. Rentsch, R. Figi, A thermodynamic and experimental study of the conditions of thaumasite formation, Cem. Concr. Res. 38 (3) (2008) 337–349.
[57] J. Bensted, Thaumasite - background and nature in deterioration of cements, mortars and concretes, Cem. Concr. Compos. 21 (2) (1999) 117–121.
[58] D.M. Mulenga, J. Stark, P. Nobst, Thaumasite formation in concrete and mortars containing fly ash, Cem. Concr. Compos. 25 (8) (2003) 907–912.
[59] M. Romer, L. Holzer, M. Pfiffner, Swiss tunnel structures: concrete damage by formation of thaumasite, Cem. Concr. Compos. 25 (8) (2003) 1111–1117.
[60] J. Bensted, Mechanism of thaumasite sulphate attack in cements, mortars and concretes, Zem.-Kalk-Gips 53 (2000) 704–709.
[61] M. Collepardi, Thaumasite formation and deterioration in historic buildings, Cem. Concr. Compos. 21 (2) (1999) 147–154.
[62] P. Pipilikaki, D. Papageorgiou, C. Teas, E. Chaniotakis, M. Katsioti, The effect of temperature on thaumasite formation, Cem. Concr. Compos. 30 (10) (2008) 964–969.
[63] S. Diamond, Thaumasite in Orange County, Southern California: an inquiry into the effect of low temperature, Cem. Concr. Compos. 25 (8) (2003) 1161–1164.
[64] P.W. Brown, R.D. Hooton, B.A. Clark, The co-existence of thaumasite and ettringite in concrete exposed to magnesium sulfate at room temperature and the influence of blast-furnace slag substitution on sulfate resistance, Cem. Concr. Compos. 25 (8) (2003) 939–945.
[65] T. Matschei, F.P. Glasser, Thermal stability of thaumasite, Mater. Struct. 48 (7) (2015) 2277–2289.
[66] I. Harris, T.J. Osborn, P. Jones, D. Lister, Version 4 of the CRU TS monthly high-resolution gridded multivariate climate dataset, Sci. Data 7 (1) (2020) 1–18.
[67] S. Sahu, S. Badger, N. Thaulow, Evidence of thaumasite formation in Southern California concrete, Cem. Concr. Compos. 24 (3–4) (2002) 379–384.
[68] C.H. Yang, B.W. Liu, X.B. Xiang, J. Zhang, The influence of pH on the formation and stability of thaumasite, Appl. Mech. Mater. 174 (2012) 268–274.
[69] K.N. Jallad, M. Santhanam, M.D. Cohen, Stability and reactivity of thaumasite at different pH levels, Cem. Concr. Res. 33 (3) (2003) 433–437.
[70] H.J. Wierig, Longtime studies on the carbonation of concrete under normal outdoor exposure, in: Proc. RILEM Seminar on the Durability of Concrete Structures Under Normal Outdoor Exposure, 1984, pp. 239–249.
[71] I. Galan, C. Andrade, M. Castellote, Natural and accelerated CO2 binding kinetics in cement paste at different relative humidities, Cem. Concr. Res. 49 (2013) 21–28.
[72] N.S. Martys, C.F. Ferraris, Capillary transport in mortars and concrete, Cem. Concr. Res. 27 (5) (1997) 747–760.
[73] M. Saeidpour, L. Wadsö, Moisture diffusion coefficients of mortars in absorption and desorption, Cem. Concr. Res. 83 (2016) 179–187.
[74] A. Leemann, F. Moro, Carbonation of concrete: the role of CO2 concentration, relative humidity and CO2 buffer capacity, Mater. Struct. 50 (1) (2017) 1–14.
[75] Met Eireann, Major Weather Events, Available at, https://www.met.ie/climate/available-data/historical-data. Accessed 13/10/2022.
[76] J. Kaufmann, Experimental Identification of Damage Mechanisms in Cementitious Porous Materials on Phase Transition of Pore Solution Under Frost Deicing Salt Attack, Swiss Federal Institut of Technology Lausanne(EPFL), 2000. Doctoral dissertation.
[77] X. Peng, W. Yimin, W. Zijian, H. Le, Distribution laws of freeze-thaw cycles and unsaturated concrete experiments in cold-region tunnels, Cold Reg. Sci. Technol. 172 (2020), 102985.
[78] J.P. Kaufmann, Experimental identification of ice formation in small concrete pores, Cem. Concr. Res. 34 (8) (2004) 1421–1427.
[79] J. Cao, D.D.L. Chung, Damage evolution during freeze–thaw cycling of cement mortar, studied by electrical resistivity measurement, Cem. Concr. Res. 32 (10) (2002) 1657–1661.
[80] R. Wang, R.Z. Hu, Y. Li, K. Wang, H. Zhang, Review on the deterioration and approaches to enhance the durability of concrete in the freeze–thaw environment, Constr. Build. Mater. 321 (2022), 126371.